

Infrared-heated Sample Introduction System to Enhance Transport Efficiency for Yeast Cell Analysis by Single Cell Inductively Coupled Plasma Mass Spectrometry

Zichao Zhou,^a Mirah J. Burgener,^b John Burgener,^b and Diane Beauchemin^{a,*}

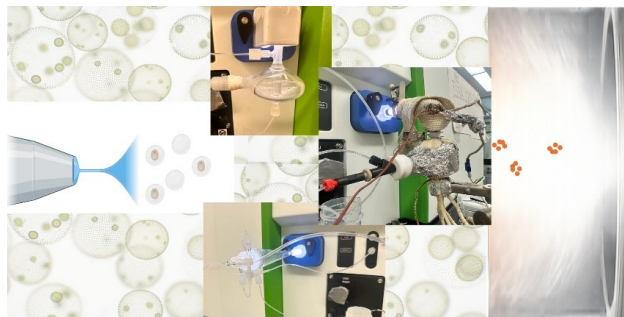
^aQueen's University, Department of Chemistry, 90 Bader Lane, Kingston, ON K7L 3N6, Canada

^bBurgener Research Inc., 2-1680 Lakeshore Rd. W, Mississauga, ON L5J 1J5, Canada

Received: April 07, 2026; Revised: May 08, 2026; Accepted: May 09, 2026; Available online: May 10, 2026.

DOI: 10.46770/AS.2026.071

ABSTRACT: Single cell inductively coupled plasma mass spectrometry (scICPMS) enables quantitative analysis of individual cells, providing access to cellular heterogeneity that is obscured in bulk analyses. However, its analytical performance is strongly constrained by sample introduction efficiency, particularly for biological cells whose transport behaviour differs from those of standard solutions and nanoparticles. In this work, an infrared (IR)-heated pneumatic sample introduction system based on a modified cyclonic spray chamber, where the aerosol is pre-evaporated without solvent removal prior to entering the plasma, was employed for scICPMS analysis of a Se-enriched *Saccharomyces cerevisiae* (yeast) certified reference material (SELM-1) while monitoring the number of detected cell events. Multivariate optimization of IR-heating temperature, nebulizer gas flow rate, sample uptake rate, and sampling position was conducted. At 150 °C and 5 $\mu\text{L min}^{-1}$ uptake rate, the IR-heated system achieved a cell transport efficiency of $47 \pm 6\%$, representing a substantial improvement compared with a conventional cyclonic spray chamber ($1.1 \pm 0.4\%$) and exceeding that of a commercial single cell introduction system ($30 \pm 3\%$). Detection limits of 100–120 ag per cell were obtained for both ^{78}Se and ^{82}Se . The Se mass per cell determined by scICPMS ($65\text{--}68 \text{ fg cell}^{-1}$) is consistent with independent estimates derived from certified total Se concentration and bulk digestion measurements, confirming analytical accuracy. Cell lysis occurred at IR-heating temperatures above 220 °C, emphasizing the necessity of optimization using cell-based matrices. Overall, this study demonstrates that controlled IR-heated sample introduction significantly enhances transport efficiency and enables reliable Se quantification in cells without requiring independent transport efficiency calibration.



INTRODUCTION

Trace metals and metalloids are indispensable to life, yet their biological functions and toxicities are frequently controlled by concentration, chemical form, and heterogeneity at the cell level. Elements such as Fe, Cu, Zn, and Se participate in core physiological processes including metabolism, redox homeostasis, cellular signalling, and gene regulation.¹ Conversely, exposure to toxic metals can perturb these same pathways and contribute to disease progression.² A fundamental limitation of conventional bulk elemental analysis is that it averages signals across thousands to millions of cells, thereby masking biologically meaningful

subpopulations and obscuring relationships between uptake, intracellular handling, and phenotype.³ This limitation is particularly problematic in contexts where only a small fraction of cells drives the overall response, for example, drug-resistant tumour subclones, rare circulating tumour cells, or a minority of highly exposed cells within an environmental population.^{4–6}

Single cell inductively coupled plasma mass spectrometry (scICPMS) enables quantitative, time-resolved acquisition of elemental signals from intact individual cells.⁷ When introducing a diluted cell suspension into scICPMS, transient signal spikes can be attributed to individual cells, enabling direct conversion of

spike intensity to analyte mass per cell and spike frequency to cell concentration under defined transport conditions. This has facilitated a fundamental shift in how elements have been measured in cells: not as a single mean value, but as a distribution reflecting heterogeneity in exposure, uptake, and intracellular processing.⁸ In practice, scICPMS can be employed to quantify two broad classes of analytes in intracellular measurements: endogenous elements present naturally in cells for the study of elemental fingerprinting and physiological profiling and exogenous elements intentionally introduced or environmentally encountered. It supports uptake and fate studies for metallodrugs,^{5,9,10} drug-transporting nanoparticles (NPs),¹¹ metal-containing NPs,¹²⁻¹⁵ and metal-tagged affinity probes.^{6,16}

Selenium is an especially compelling target for advancing scICPMS methodology. As an essential trace element involved in antioxidant defence and immune function, Se is widely studied in nutritional and toxicological research. Organic Se species like selenomethionine (produced by organisms such as *Saccharomyces cerevisiae*) are valued for their comparatively high bioavailability and low toxicity, motivating accurate measurement and speciation of Se in yeast-based supplements and reference materials.¹⁷⁻²² The availability of SELM-1 Se-enriched yeast cell certified reference material (CRM) enabled intracellular versus extracellular Se determinations and facilitated the development of scICPMS.^{19,21} However, Se determination by ICPMS is frequently challenged by spectroscopic interferences (Table S1), which can be mitigated using a collision/reaction cell or tandem mass spectrometry,²⁰ but at the expense of sensitivity. One way to compensate for this is to use a sample introduction system providing improved transport efficiency (TE) as this increases sensitivity for measurement of dissolved analyte while allowing more cells to be analyzed by scICPMS within a given period.

Accurate quantification in scICPMS depends on reliable TE determination.²³ However, most scICPMS methods rely on TE determined by using NPs suspensions for determination of cell concentration despite the fact that NPs (typically <100 nm) and cells (as large as ~10 µm in the case of mammalian cells) may exhibit substantially different transport behaviour. Recent comparative studies have underscored that suitable calibrants, including cell-based CRMs, are essential for accurate determination of cell concentration in scICPMS.²² Eliminating the requirement for TE measurement altogether would be advantageous, particularly in high-throughput applications involving large sample numbers or multiple elements. In single particle ICPMS (spICPMS), integrating the signal instead of averaging it²⁴ or using flow injection²⁵ or monosegmented flow analysis²⁶ for sample injection (with integration of the injection peak) avoids this requirement when NP size or mass is being determined but TE must be measured if NP concentration is also desired. Measurement of TE would be avoided altogether with a total-consumption sample introduction system.

Sample introduction thus remains a principal determinant of measurement quality in scICPMS as cells must be introduced in a manner compatible with time-resolved ICPMS detection while preserving their integrity. Table S2 summarizes different sample introduction systems that have been used for scICPMS. Several heated or temperature-controlled sample introduction systems are commercially available. These include desolvating systems such as the ESI Apex series and Teledyne CETAC Aridus3, as well as temperature-controlled spray chambers such as the Glass Expansion IsoMist and ESI PC³. These systems can improve sensitivity and signal stability, enhance solvent removal, and reduce oxide interferences. However, solvent removal conversely reduces the beneficial load buffer effect of water on the plasma, which exacerbates matrix effects.

In any case, Table S2 reveals that total-consumption and micro-flow introduction systems can substantially increase TE and reduce sample consumption.²⁷⁻²⁹ With many systems however, TE is under 5%, which does not provide a complete picture of the sample composition. Even using computational fluid dynamics to design a 3D-printed total consumption system yielded TE of 61% for Au NPs at 10 µL min⁻¹ and 80 °C.³⁰ Increasing spray chamber temperature can improve TE for large mammalian cells.³¹ However, even when a spray chamber designed for scICPMS was heated to 120°C, only 27% TE was achieved for mammalian cells.³² The few systems in Table S2 that provide 100% TE are not commercially available and use a nebulizer known to be prone to blockage. Furthermore, all the heated systems involved convective heating, which is not as efficient as infrared (IR) heating and prone to memory effects.³³

The aim of this work was to explore the performance of a system employing a parallel path nebulizer, which is not prone to blockage, in combination with an IR-heated modified cyclonic spray chamber for scICPMS. This system was reported to improve TE in spICPMS.³⁴ Although IR heating conditions were optimized along with the nebulizer gas flow rate for 100% TE of Au and Pt NPs,³⁵ the system has not yet been used for scICPMS. The goal of the present work was to study the effect of IR heating temperature, sample uptake rate over the range normally used with a commercially available system to enable direct comparison to it, sampling position, and nebulizer gas flow rate on sensitivity and TE in scICPMS. Multivariate optimization was performed using a cell suspension rather than a Se standard solution. Like sample introduction systems using heaters in Table S2, reducing droplet size via controlled pre-evaporation is expected to increase TE and improve the signal-to-noise ratio and thus the detection limit. Ultimately, this work aims to advance practical, high accuracy scICPMS determination of Se in selenized yeast, supporting both instrumental development and broader applications in nutrition, supplement quality control, and Se toxicology.

Table 1. Operating conditions for scICPMS

Spray chamber type and nebulizer	Standard cyclonic and Burgener SC175	Asperon™ and Meinhard high efficiency glass concentric nebulizer	IR-heated modified cyclonic and Burgener SC175
Ar plasma gas flow rate (L min ⁻¹)	15.0	15.0	15.0
Ar auxiliary gas flow rate (L min ⁻¹)	1.20	1.20	1.20
RF power (kW)	1.60	1.60	1.60
Ar nebulizer gas flow rate (L min ⁻¹)	0.98	0.36	0.99
Ar aerosol dilution ¹ gas flow rate (L min ⁻¹)	0	0.7	Not applicable
Sampling position ²	0	0	-3
Operation temperature (°C)	20	20	150
Sample uptake rate (μL min ⁻¹)	5	5	5
Dwell time (μs)	50	50	50

¹ Aerosol dilution was carried out via the “All Matrix Solution” port of the PerkinElmer spray chamber. ² 0 is a default position for PE NexION 2000; adjustable range from -3 to 3.

EXPERIMENTAL

Instrumentation. A NexION 2000 ICPMS instrument (PerkinElmer, Waltham, MA, USA) equipped with Syngistix single cell analysis software was employed without any collision or reaction gas to maximize sensitivity during measurement of dissolved analyte resulting from cell lysis. To check for the effect of spectroscopic interference, such as that of ³⁸Ar⁴⁰Ca⁺ on ⁷⁸Se⁺, ⁸²Se⁺ was also monitored to verify that the same results as with ⁷⁸Se⁺ were obtained. For optimization, solutions and cell suspensions were introduced at 5 to 25 μL min⁻¹ using a standalone peristaltic pump. There was no evidence of pulsation in the blank signal or the cell suspension signal (Fig. S1). Sample uptake rate was verified from the weight difference of a double deionized water (DDW) container after aspirating DDW for 5 min. Cytoflex flow cytometry (Beckman, Indianapolis, IN, USA) was used to independently count the washed cells and determine a cell number concentration.

The IR-heated sample introduction system (Fig. S2) was as described previously,³⁴ with only the nebulizer changed to an SC175 (Burgener Research Inc., Mississauga, ON, Canada) designed for low-flow operation in scICPMS. The system consisted of a 50-mL modified baffled cyclonic spray chamber with a 2-mm gap between the top of the modified baffle and the top service of the spray chamber, a shortened neck and an L-shaped elbow (JRV Scientific Glass, Montreal, QC, Canada). It was attached to the base of the ICP torch using a custom-made connector made of an open-end male ball joint and a polytetrafluoroethylene sleeve (SCP Science, Baie d’Urfé, QC, Canada). Heating was done using a ceramic rod IR heater with an integrated thermocouple (Elstein-Werk, Northheim, Germany) inserted into the modified baffle, and a ceramic beaded rope IR heater (Marsh Beaded Heaters, Normangee, TX, USA) wrapped around the elbow connection and base of the torch, with an additional thermocouple inserted underneath the IR rope heater, which were connected to two identical DigiTrol II temperature

controllers (GLAS-COL Apparatus Company, Terre Haute, IN, USA). The entire assembly was insulated with glass-fibre heat-resistant tape and aluminium foil. Such a system pre-evaporates the aerosol while preserving water vapour that acts as a load buffer in the plasma.

For comparison, two commercial nebulization systems were used: an SC175 nebulizer in a baffled cyclonic C3 high-sensitivity glass cyclonic spray chamber with a matrix gas port (PerkinElmer) and a high efficiency glass concentric nebulizer (Meinhard, Golden, CO, USA) in an Asperon™ spray chamber (PerkinElmer), which is a single pass spray chamber designed for scICPMS. Operating conditions with the different systems are summarized in Table 1. To determine the Se concentration in cell digests and cell washings, bulk analysis was carried out using external calibration with conventional ICPMS employing the operating conditions in Table 1, but with a dwell time of 10 ms.

Chemicals. Se standard solutions for external calibration were prepared in 2% v/v HNO₃ from 10000 mg L⁻¹ Se solutions (SCP Science), sub-boiled HNO₃ and DDW (18.2 MΩ cm) (Arium Pro UV/DI System, Sartorius Stedim Biotech, Goettingen, Germany). Similarly, a 1 ng mL⁻¹ multielement tuning solution was prepared from ICPMS stock tuning solution and used to optimize the performance of the cyclonic and Asperon™ spray chambers systems. A DST-1000 sub-boiling distillation system (Savillex, Minnetonka, MN, USA) was used to purify HNO₃ (ACS grade; Fisher Scientific, Ottawa, ON, Canada). DDW was passed through a 0.22 μm syringe filter (Sigma Aldrich, Burlington, MA, USA) to remove potential bacteria and microplastics that might interfere with flow cytometry and scICPMS. Se-enriched yeast SELM-1 CRM (National Research Council Canada, Ottawa, ON, Canada) was used for method development because of the unavailability of cell CRMs containing interference-free elements like Ag or Pt.

A suspension of certified Au NPs in water (99.99% purity;

diameter of 60.6 ± 5.9 nm) from nanoComposix (San Diego, CA, USA) was used to measure NPs TE. These NPs were stabilized in citrate buffer and have a near spherical geometry. Certified NP suspensions were diluted to 100000 particles mL^{-1} with DDW to ensure that each droplet produced during nebulization would contain at the most one NP. To avoid NP dissolution and aggregation, dilution was performed on the day of the analysis followed by sonication for 10 min prior to analysis.

Cells treatment. A Se-enriched yeast cell suspension was prepared from SELM-1 CRM, with a certified total Se concentration of 2031 ± 70 mg kg^{-1} . The tube was sonicated for 3 min in an ultrasonic bath (Ultrasons 30000514, J.P. Selecta, Barcelona, Spain) prior to scICPMS analysis. For ICPMS analyses, to remove extraneous Se, the tube was centrifuged at 5000 rpm for 10 min (Fisher scientific, Hampton, New Hampshire, United States). After collecting the supernatant, another 50 mL of filtered DDW was added and suspension was ensured using a Vortex-Genie 2 (Scientific industries, Inc., Bohemia, NY, USA) prior to centrifugation to collect the washing. Cells cleaning was repeated three times in total. The total extracellular Se content was determined by summing the total Se concentration measured in three cell washes by ICPMS and the background Se signal obtained by scICPMS. The washing solution at each stage was collected and diluted 100-fold prior to analysis by ICPMS.

Digestion. To determine the intracellular Se content by ICPMS, a simple acid digestion was performed.³⁶ The washed cells were added to 5 mL of concentrated HNO_3 and soaked overnight. Then, the mixture was heated to 90 °C in a water bath for 4 h. The digest was finally diluted to 50 mL with DDW for analysis by ICPMS.

Optimization. A multivariate optimization was performed of the nebulizer gas flow rate (0.9 - 1.1 L min^{-1} range), sample uptake rate (5 - 25 $\mu\text{L min}^{-1}$ range), IR heating temperature (20 - 150 °C range), and sampling position (-3 to $+3$, controlled by the NexION software). The range of sample uptake rate was that normally used with the Asperon™ system to enable a direct comparison. A $(1.96 \pm 0.09) \times 10^5$ cells mL^{-1} suspension, confirmed by flow cytometry, was used to this end. A central composite design was generated with Minitab 18 (State College, Pennsylvania, USA) statistical software (Table S3).

Single cell measurement. Data acquisition was in time-resolved analysis mode during 100 s with a dwell time of 50 μs while monitoring ^{78}Se , ^{82}Se or ^{24}Mg . As the average signal duration per cell was approximately 300-500 μs , a dwell time of 50 μs was selected to provide enough data points across each cell event without generating an excessive number of points for data processing. As Mg is a constitutive element of cells,³⁵ it can be used as an internal cell marker. Cell events were identified as data points whose intensity was above the mean of the entire data set by over 3 times the standard deviation. The identified cell events

were removed, and the same process was repeated with the remaining data until there were no data points higher than the mean plus 3σ . The remaining data points constituted the background signal of the cell suspension. The above identification method was also applied to NPs suspensions.

The amount of Se in individual cells was determined by using an external calibration with Se standard solutions (0.1 - 100 ng L^{-1}), where the mass flux on the x-axis was obtained by multiplying the Se concentration by solution TE (assumed to be equal to NPs TE), the uptake rate and the dwell time. This approach can be used to find the mass of Se in individual cells, irrespectively of the lower TE for cells, which affects cell concentration in solution, not the amount of Se in cells. Using the calibration, the intensity of each transient cell event signal was converted to Se mass per cell. Binning the calculated masses from all detected cell events based on frequency yielded the Se mass distribution in the cells, which was fitted to a lognormal model. The acquired data were further processed using Excel 365 (Microsoft) and GraphPad Prism 9 (GraphPad Software 225, Boston, MA, USA).

The detection limit for dissolved analyte was determined from the standard deviation of 10 replicate measurements of DDW and converted to a concentration detection limit using an external calibration. The absolute detection limit was then calculated from this concentration detection limit by applying the mass flux and converting the result to mass.

Measurement of transport efficiency. The measurement of NPs TE was done by spICPMS while introducing a NPs suspension of known concentration under identical conditions to those employed for scICPMS in Table 1. The ratio of detected NP events to the total number of NPs delivered to the sample introduction system during the measurement period corresponded to TE. Similarly, the ratio of detected cell events over the total number of nebulized cells corresponded to cells TE. TE was normalized based on the ratio of the average number of detected cell signals from the two Se isotopes to the number of detected Mg signals (Fig S3).

RESULTS AND DISCUSSION

Multivariate optimization. The objective of the multivariate optimization was to maximize the number of cell events detected during the nebulization of a washed cell suspension of constant concentration at sample uptake rates typically used for the measurement of cells (Table S2). The number of detected cell events was normalized to the sample uptake rate, yielding TE per unit volume introduced and enabling comparison across conditions. A cell concentration of 2×10^5 cells mL^{-1} was selected as it was the highest cell concentration yielding a proportional increase in cell event frequency with minimal change in average

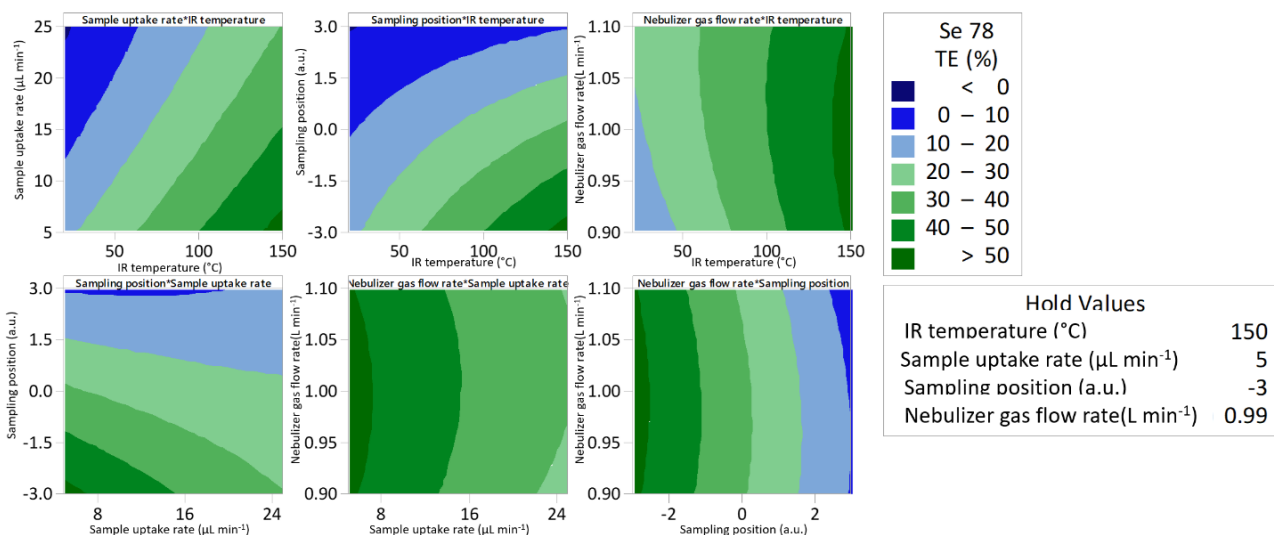


Fig. 1 Contour plots of ^{78}Se cell TE from a $1.96 \pm 0.09 \times 10^5$ cells mL^{-1} SELM-1 suspension in DDW under different operating conditions.

Table 2. Figures of merit for three sample introduction systems in scICPMS

Spray chamber type and nebulizer	Standard cyclonic and Burgener SC175	Asperon™ and Meinhard high efficiency glass concentric nebulizer	IR-heated modified cyclonic and Burgener SC175
Sensitivity for ^{78}Se (cps μg^{-1})	$(1.40 \pm 0.4) \times 10^9$	$(5.1 \pm 1) \times 10^9$	$(5 \pm 2) \times 10^9$
Detection limit for ^{78}Se ($\mu\text{g L}^{-1}$)	10	3	3
Absolute detection limit for ^{78}Se (fg)	0.4	0.1	0.1
Sensitivity for ^{82}Se (cps μg^{-1})	$(6.04 \pm 0.4) \times 10^8$	$(2.03 \pm 0.5) \times 10^9$	$(1.7 \pm 0.7) \times 10^9$
Detection limit for ^{82}Se ($\mu\text{g L}^{-1}$)	8	3	3
Absolute detection limit for ^{82}Se (fg)	0.3	0.08	0.1
Cell transport efficiency (%)	1.1 ± 0.4	30 ± 3	47 ± 6

cell event intensity (Fig. S4). This concentration is much lower than the theoretical 2×10^7 cells mL^{-1} calculated using $5 \mu\text{L min}^{-1}$ while assuming 100% TE and allowing 500 μs per cell to avoid overlap. Signal overlap due to coincident events would suddenly increase the average signal intensity of cell events beyond a certain cell concentration. The presence of individual cells was also confirmed by flow cytometry (Fig. S5).

Two independent multivariate optimizations were conducted, targeting the ^{78}Se and ^{82}Se isotopes, respectively. As expected, similar results were obtained for both isotopes (Fig. 1 and Fig. S6). As the concentration of the cell suspension was kept constant throughout, the number of detected cell events is proportional to TE.

As temperature increased from 20 °C to 150 °C, the number of detected cells increased substantially (Fig. 1). Additionally, higher TE resulted when the torch was positioned closer to the sampler cone, indicating that pre-evaporation leaves more energy to the plasma for the atomization and ionization processes, which occur sooner in the plasma. At lower sample uptake rates, the aerosol underwent more effective pre-evaporation, resulting in a greater proportion of the introduced sample reaching the plasma per unit volume. Nebulizer gas flow rate exhibited the least pronounced

effect on TE, with similar cell counts across a nebulizer gas flow rate range of 0.95–1.10 L min^{-1} . No cell lysis occurred in the range of nebulizer gas flow rates tested as cell events resulted without any significant increase in background signal that would indicate cell lysis.

Fig. S7 indicates that temperature has the largest standardized effect for both ^{78}Se and ^{82}Se , with sample uptake rate and sampling position also having a significant but lesser effect. The temperature range of 20 °C to 150 °C for the optimization was selected based on past studies (Table S2). The conditions statistically maximizing the TE for both isotopes were computed by Minitab 18 and are summarized in Table 1. They were used thereafter, except where otherwise specified. The selected temperature of 150 °C corresponds to the highest temperature used in past studies (Table S2).

Figures of merit. Table 2 compares the analytical performance obtained with the IR-heated system to that from two commercially available sample introduction systems. All measurements were conducted at an identical sample uptake rate of $5 \mu\text{L min}^{-1}$ to allow a direct comparison of sensitivity, detection limits, and TE. Compared to the standard cyclonic system, the Asperon™ system operated at 20 °C and the IR-heated sample introduction system at

Table 3. Intracellular and extracellular Se concentrations measured directly for 2.11×10^5 unwashed cells mL^{-1} by scICPMS using two Se isotopes with two sample introduction systems ($n=3$ separate analyses)

Sample introduction system	Intracellular Se (mg kg^{-1})	Extracellular Se (mg kg^{-1})	Total Se (mg kg^{-1})
IR-heated (^{78}Se)	1600 ± 400	600 ± 200	2200 ± 400
IR-heated (^{82}Se)	1400 ± 200	400 ± 80	1800 ± 200
Asperon TM (^{78}Se)	1200 ± 200	700 ± 90	1900 ± 200
Asperon TM (^{82}Se)	1260 ± 40	680 ± 20	2000 ± 40

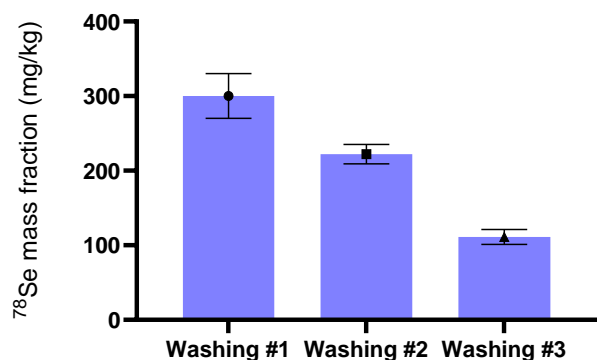


Fig. 2 Extracellular Se concentration measured during successive washings of a SELM-1 suspension (error bars are standard deviations for $n=3$ separate analyses).

150 °C yielded a 2- to 4-fold improvement in sensitivity for both ^{78}Se and ^{82}Se . This increase in sensitivity cannot be attributed to an increase in Ar_2^+ background, which was lowest with the AsperonTM system and roughly doubled upon switching from a standard cyclonic spray chamber to the IR-heated system (Fig. S1), commensurate with the hotter plasma resulting from the introduction of vaporized instead of wet aerosol. A difference in droplet size distribution exiting the spray chamber may explain why the background with the cyclonic spray chamber is roughly doubled that with the AsperonTM system as both were operated at room temperature. The enhancement in sensitivity stems from a marked increase in TE, from $1.1 \pm 0.4\%$ with the cyclonic spray chamber to $30 \pm 3\%$ with the AsperonTM system, and $47 \pm 6\%$ with the IR-heated system.

Despite the highest TE with the IR-heated system, sensitivities for both Se isotopes were comparable to those obtained with the AsperonTM system because a greater variability in signal and background was observed (Fig. S1). This was also reflected in the detection limits, which were similar to those with the AsperonTM system and improved relative to the standard cyclonic spray chamber. Hence, elevated TE does not necessarily translate into proportionally improved detection limits when additional sources of signal variability are present. Enhancing the precision and stability of the IR-heated sample introduction system will be the aim of future work. Although the sensitivity ratio of the two Se isotopes matches their isotopic abundance ratio, the averaged

background signal and associated standard deviation were higher for ^{78}Se because $^{38}\text{Ar}^{40}\text{Ar}^+$ is more abundant than $^{40}\text{Ar}_2^+\text{H}_2^+$. This resulted in a better detection limit for ^{82}Se despite its lower sensitivity.

Nonetheless, under the conditions in Table 1, the IR-heated sample introduction system provided $100 \pm 10\%$ TE for solutions and NPs as opposed to $9 \pm 2\%$ and $79 \pm 5\%$ with the cyclonic spray chamber and the AsperonTM system respectively. The total consumption with the IR-heated system is as expected from previous work where 100% TE was also achieved at a higher sample uptake rate (50 instead of $5 \mu\text{L min}^{-1}$) and lower temperature (110 instead of 150 °C).³⁵ Given that neither of the other two systems provided 100% TE for solutions and NPs, the IR-heated system is clearly more universal.

SELM-1 measurements. To validate the performance of the IR-heated sample introduction system for scICPMS, complementary analyses were performed: direct scICPMS measurement of cells and extracellular Se content as well as ICPMS determination of extracellular and intracellular Se following washings of cells and cells digestion respectively. For all Se determinations, calibration was performed using dissolved Se standard solutions.

The results obtained by scICPMS using the IR-heated sample introduction system and the AsperonTM system designed for scICPMS are summarized in Table 3 for the intracellular Se measured in cellular events and the extracellular Se left in the background after removing cellular events. All the results agree with the certified Se concentration of $2030 \pm 70 \text{ mg kg}^{-1}$ according to a Student's *t* test at the 95% confidence level. These results were obtained despite only measuring during 100 s for each replicate.

In contrast, intracellular Se content was determined by ICPMS after washing the cell suspension three times to remove extracellular Se species, which took nearly 1 h. Fig. 2 shows that extracellular Se concentration decreased progressively across successive washing fractions. However, residual Se was still detectable in the final washing fraction, suggesting that additional washing steps may be required to achieve more complete removal of extracellular Se and, consequently, more accurate quantification of intracellular Se content. The general agreement between the ICPMS results and the scICPMS ones for extracellular Se indicates that cell washing did not release a significant amount of intracellular Se.

Nonetheless, the experimentally determined 72% of total Se present in the washed cells (Table 4) and the 63-77% of total Se measured in cells by scICPMS are consistent with previous reports of 50-75% of total Se being present in intracellular form.^{19,21} Table 4 also shows that mass balance was verified as the sum of intracellular and extracellular Se concentrations matched the certified total Se concentration, with a total Se recovery of 99-103%.

Table 4. Intracellular and extracellular Se concentrations measured by ICPMS using two Se isotopes with the IR-heated sample introduction system (n=3)

Sample Fraction	Mass Fraction (mg kg ⁻¹)
Digested washed cells (⁷⁸ Se)	1460 ± 90
Digested washed cells (⁸² Se)	1470 ± 90
Washed cells + 3 washings (⁷⁸ Se)	2100 ± 100
Washed cells + 3 washings (⁸² Se)	2000 ± 100
CRM certified Se concentration	2030 ± 70

Table 5. Se mass per cell measured with IR-heated sample introduction system (n=3 separate analyses)

	Se concentration (fg cell ⁻¹)
Se in SELM-1 ¹	70.3
Se in SELM-1 measured with ⁷⁸ Se	66 ± 5
Se in SELM-1 measured with ⁸² Se	68 ± 6

¹ Calculated using the certified total Se concentration.

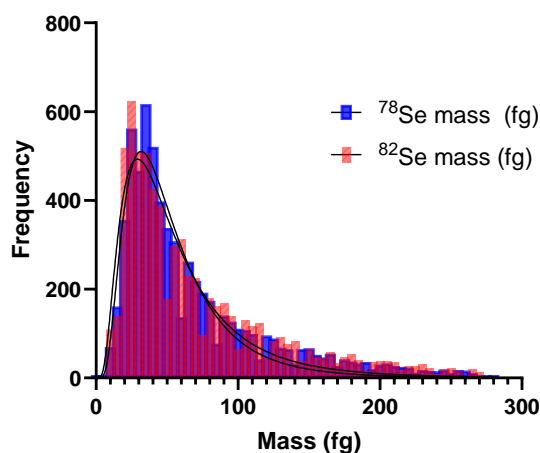


Fig. 3 Mass distribution of Se yeast cells of SELM-1 measured by scICPMS with optimized IR-heated sample introduction system.

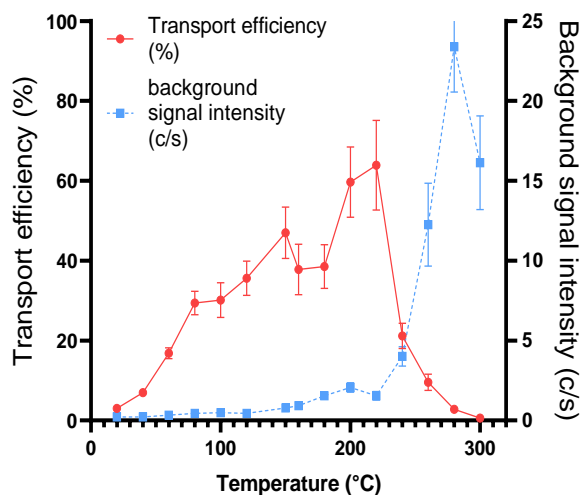


Fig. 4 Transport efficiency measured at 50 μL min⁻¹ while monitoring ⁸²Se for a SELM-1 suspension and dissolved background signal obtained with the IR-heated sample introduction system at different temperatures (n=3).

However, the time required to prepare samples for ICPMS analyses (nearly 1 h for 3 washings plus overnight digestion of washed cells and heating at 90 °C for 4 h) greatly exceeds the 300 s in total taken for 3 replicate scICPMS analyses. The only drawback of scICPMS is that the extensive dilution required to ensure one cell per droplet at the most may bring the dissolved Se concentration close to the determination limit.

The Se content per cell obtained by scICPMS is reported in Table 5. Because the error for one replicate analysis of 700-800 cells was quite large, such as an averaged mass of 67 ± 50 fg using ⁸²Se and 69 ± 52 fg using ⁷⁸Se, the average of 3 replicate analyses is reported in Table 5. Values determined using ⁷⁸Se and ⁸²Se are in agreement, according to a Student's t test at the 95% confidence level. They also agree with an independent estimate of Se mass per cell calculated using the certified total Se concentration, the known cell number concentration, and the ratio of Mg-associated cell events to Se-associated cell events. Specifically, the certified Se content per cell was estimated by subtracting the extracellular Se concentration measured by ICPMS from the certified total Se content and then normalizing the remaining Se to the total cell count number of Se-containing cells. The measured cell contents also agree with published Se mass per cell for the same CRM, which ranges from approximately 40 to 70 fg per cell.¹⁹⁻²¹ As expected, the mass distributions obtained using the two Se isotopes substantially overlap (Fig. 3). In fact, a Kolmogorov-Smirnov test indicated no significant difference between them. Hence, both isotopes allow accurate quantification of Se in the yeast CRM, confirming that any spectroscopic interference does not impede accurate analysis without a collision or reaction gas.

The above results were obtained at a sample uptake rate of 5 μL min⁻¹, as used with standard single cell spray chambers (Table S2). However, the temperature with the IR-heated system was the highest tested. The 20-150 °C range was selected based on reports that yeast cells underwent lysis at 45-90 °C.^{36,37} As 150 °C is above the temperature providing 100% TE in spICPMS,^{34,35} a test was conducted under spICPMS conditions to explore whether further improvements could be achieved.

Optimization under spICPMS conditions. The IR heating temperature was varied while maintaining a sample uptake rate of 50 μL min⁻¹, consistent with the conditions previously employed for total consumption NP analysis.³⁴ When the Se-enriched yeast cell suspension was introduced, TE measured using ⁸²Se increased substantially with temperature, rising from approximately 1% at room temperature to 60% at 220 °C (Fig. 4). However, upon a further increase in temperature, the number of detected cell events declined markedly, down to 0.5% TE at 300 °C. Concurrently, the background Se signal remaining after cell event identification increased approximately 10-fold. This indicates the occurrence of cell lysis, which released intracellular Se into the carrier solution. There is thus an upper temperature for cells suspension

introduction, unlike with standard solutions, which is significantly higher than expected based on bulk heating of yeast cells.

This suggests that water may preferentially absorb IR energy and be evaporated from droplets, allowing the cells to remain intact. A wider range of temperatures should be tested as it may be possible to achieve 100% TE for cells (as well as NPs) at a higher temperature than 150 °C and a lower uptake rate than 50 $\mu\text{L min}^{-1}$. For scICPMS applications, optimization of IR heating conditions should be performed using cell suspensions of comparable composition to the samples of interest, rather than relying solely on dissolved elemental standards. Indeed, the optimal conditions likely depend on the cell type. For instance, yeast cells possess a higher thermotolerance than eukaryotic cells because of their different cell wall.³⁹ The conditions used in this work for Se-enriched yeast cells may thus not be applicable to other cell types, such as eukaryotic cells, because an increase in temperature may enhance membrane permeability, promoting intracellular element release, or cause cell lysis.⁴⁰ Thus, temperature optimization in scICPMS should balance improved TE with preservation of cell integrity and analyte retention.

CONCLUSION

This study demonstrates that IR-heated pneumatic sample introduction provides an effective strategy for improving TE and analytical performance in scICPMS. By systematically optimizing instrumental parameters using a Se-enriched yeast cell suspension rather than dissolved standards, conditions were identified that substantially increased the fraction of cells delivered to the plasma while preserving them. At a sample uptake rate of 5 $\mu\text{L min}^{-1}$ typically used in scICPMS, the IR-heated system achieved nearly 50% cell TE. This is an improvement of more than an order of magnitude over a conventional cyclonic spray chamber system and significantly higher than a commercial single cell introduction device operated at room temperature. The IR-heated system simultaneously achieved total consumption for solutions and NPs, which the other systems tested did not. A further increase in TE may be possible with an increase in temperature up to 220 °C, as 60% TE was achieved at 220 °C but at 50 $\mu\text{L min}^{-1}$. A higher TE may be possible at a lower sample uptake rate, such as 5 $\mu\text{L min}^{-1}$ typically used for scICPMS. Multivariate optimization over a larger range of heating temperatures will be conducted in future work.

Accurate Se quantification in cells was achieved for the SELM-1 CRM, with measured Se masses per cell in agreement with values calculated from certified bulk composition and with literature reports. Importantly, temperature-dependent experiments revealed that optimization based solely on dissolved standards can be misleading for biological samples. Excessive heating would induce cell lysis, thereby redistributing intracellular analytes into

the dissolved background and degrading cell detectability.

Taken together, these findings highlight the critical role of sample introduction design in scICPMS and establish IR-heated pneumatic sample introduction as a practical approach for enhancing TE and providing accurate measurement in cell elemental analysis. The methodology developed here is readily applicable to other trace elements and biological systems and should allow routine analysis of other kinds of cells.

Future work will check if using ^{80}Se along with a light reaction gas (H_2) to reduce the interference from $^{40}\text{Ar}_2^+$ would be more effective than monitoring less abundant Se isotopes in no-gas mode. Optimizations will also be conducted with different cell types, including mammalian and bacterial cells, and different elements to investigate how optimal operating conditions vary based on the cell type and establish how universal the IR-heated sample introduction system really is.

ASSOCIATED CONTENT

The data supporting this article (Tables S1-S3 and Figs. S1-S7) is available at <https://www.at-spectrosc.com>

AUTHOR INFORMATION



Diane Beauchemin received her Ph.D. in 1984 from l'Université de Montréal. She is a professor (Full) and Undergraduate Chair at Queen's University. Her research efforts are focused on inductively coupled plasma mass spectrometry (ICPMS) and ICP optical emission spectrometry (OES) from both fundamental and application perspectives, and expanding the range of

application of ICPMS/OES to geochemical exploration, risk assessment of food safety, characterization of nanoparticles, and forensic analysis. She has been working as member of editorial board for Atomic Spectroscopy. Diane Beauchemin won the Alan Date Memorial Award (1988) from VG Elemental, the Distinguished Service Award (2001) from Spectroscopy Society of Canada, the Maxxam Award (2017) and Clara Benson Award (2019) from Canadian Society for Chemistry, the Gerhard Herzberg Award (2018) from the Canadian Society for Analytical Sciences and Spectroscopy, and the 2024 Environment Division Research and Development Dima Award from the Chemical Institute of Canada. She is author or coauthor of over 190 articles published in peer-reviewed scientific journals.

Corresponding Author

* D. Beauchemin

Email address: diane.beauchemin@queensu.ca

Notes

There are no conflicts to declare. Although Burgener Research provided input into the research as well as funding to support ZZ, they currently have no plan to commercialize the proposed system.

ACKNOWLEDGMENTS

The authors gratefully acknowledge the financial support of the Natural Sciences and Engineering Research Council of Canada (grant number 578516-22) and of Mitacs (grant number IT33380). ZZ also thanks Queen's School of Graduate Studies for a graduate award and is grateful to Burgener Research for internship support.

REFERENCES

1. P. D. Whanger, *J. Trace Elem. Exp. Med.*, 1998, **11**, 227–240. [https://doi.org/10.1002/\(SICI\)1520-670X\(1998\)11:2/3%253C227::AID-JTRA13%253E3.0.CO;2-T](https://doi.org/10.1002/(SICI)1520-670X(1998)11:2/3%253C227::AID-JTRA13%253E3.0.CO;2-T)
2. H. Koyama, T. Kamogashira and T. Yamasoba, *Antioxidants*, 2024, **13**, 76. <https://doi.org/10.3390/antiox13010076>
3. G.-C. Yuan, L. Cai, M. Elowitz, T. Enver, G. Fan, G. Guo, R. Irizarry, P. Kharchenko, J. Kim, S. Orkin, J. Quackenbush, A. Saadatpour, T. Schroeder, R. Shivdasani and I. Tirosh, *Genome Biol.*, 2017, **18**, 84. <https://doi.org/10.1186/s13059-017-1218-y>
4. A. B. S. da Silva and M. A. Z. Arruda, *Trace Elem. Med. Biol.*, 2023, **75**, 127086. <https://doi.org/10.1016/j.temb.2022.127086>
5. T. Liu, E. Bolea-Fernandez, C. Mangoldt, O. De Wever and F. Vanhaecke, *Anal. Chim. Acta*, 2021, **1177**, 338797. <https://doi.org/10.1016/j.aca.2021.338797>
6. Y. Xu, B. Chen, M. He, Z. Cui and B. Hu, *Anal. Chem.*, 2023, **95**, 14061–14067. <https://doi.org/10.1021/acs.analchem.3c02680>
7. L. Mueller, H. Traub, N. Jakubowski, D. Drescher, V. I. Baranov and J. Kneipp, *Anal. Bioanal. Chem.*, 2014, **406**, 6963–6977. <https://doi.org/10.1007/s00216-014-8143-7>
8. M. Resano, M. Aramendía, E. García-Ruiz, A. Bazo, E. Bolea-Fernandez and F. Vanhaecke, *Chem. Sci.*, 2022, **13**, 4436–4473. <https://doi.org/10.1039/D1SC05452J>
9. M. Corte Rodríguez, R. Álvarez-Fernández García, E. Blanco, J. Bettmer and M. Montes-Bayón, *Anal. Chem.*, 2017, **89**, 11491–11497. <https://doi.org/10.1021/acs.analchem.7b02746>
10. A. Galé, L. Hofmann, N. Lüdi, M. N. Hungerbühler, C. Kempf, J. T. Heverhagen, H. Von Tengg-Koblighk, P. Broekmann and N. Ruprecht, *IJMS*, 2021, **22**, 9468. <https://doi.org/10.3390/ijms22179468>
11. L. Gutierrez-Romero, B. Gallego, E. Blanco, U. Karst, R. Rodríguez and M. Montes-Bayon, *Anal. Chim. Acta*, 2025, **1336**, 343462. <https://doi.org/10.1016/j.aca.2024.343462>
12. M. Bakir, I. Abad-Alvaro, F. Laborda and V. I. Slaveykova, *Aquat. Toxicol.*, 2025, **286**, 107430. <https://doi.org/10.1016/j.aquatox.2025.107430>
13. W. Tang, B. Chen, M. He, G. Song, Y. Bi and B. Hu, *Anal. Chem.*, 2024, **96**, 17831–17839. <https://doi.org/10.1021/acs.analchem.4c04305>
14. M. Melczer, J. Jiménez Lamana, A. Justo-Vega, O. Hanser, S. Ndaw and R. Lobinski, *Talanta*, 2024, **267**, 125226. <https://doi.org/10.1016/j.talanta.2023.125226>
15. A. Justo-Vega, R. Domínguez-González, P. Bermejo-Barrera, A. Moreda-Piñeiro and J. Jiménez-Lamana, *Talanta*, 2026, **298**, 128972. <https://doi.org/10.1016/j.talanta.2025.128972>
16. X. Zhang, X. Wei, C.-X. Wu, X. Men, J. Wang, J.-J. Bai, X.-Y. Sun, Y. Wang, T. Yang, C. T. Lim, M.-L. Chen and J.-H. Wang, *ACS Nano*, 2024, **18**, 6612–6622. <https://doi.org/10.1021/acsnano.3c12803>
17. Z. Mester, S. Willie, L. Yang, R. Sturgeon, J. A. Caruso, M. L. Fernández, P. Fodor, R. J. Goldschmidt, H. Goenaga-Infante, R. Lobinski, P. Maxwell, S. McSheehy, A. Polatajko, B. B. M. Sadi, A. Sanz-Medel, C. Scriver, J. Szpunar, R. Wahlen and W. Wolf, *Anal. Bioanal. Chem.*, 2006, **385**, 168–180. <https://doi.org/10.1007/s00216-006-0338-0>
18. E. Rampler, S. Rose, D. Wieder, A. Ganner, I. Dohnal, T. Dalik, S. Hann and G. Koellensperger, *Metallomics*, 2012, **4**, 1176–1184. <https://doi.org/10.1039/c2mt20138k>
19. J. S. F. Pereira, R. Álvarez-Fernández García, M. Corte-Rodríguez, A. Manteca, J. Bettmer, K. L. LeBlanc, Z. Mester and M. Montes-Bayón, *Talanta*, 2023, **252**, 123786. <https://doi.org/10.1016/j.talanta.2022.123786>
20. R. Álvarez-Fernández García, M. Corte-Rodríguez, M. Macke, K. L. LeBlanc, Z. Mester, M. Montes-Bayón and J. Bettmer, *Analyst*, 2020, **145**, 1457–1465. <https://doi.org/10.1039/C9AN01565E>
21. A. Bazo, E. Bolea-Fernandez, A. Rua-Ibarz, M. Aramendía and M. Resano, *Anal. Chem.*, 2025, **97**, 13922–13929. <https://doi.org/10.1021/acs.analchem.5c01588>
22. A. Suárez Priede, M. Corte-Rodríguez, H. Gödde, M. Montes Bayón and J. Bettmer, *Talanta*, 2025, **295**, 128372. <https://doi.org/10.1016/j.talanta.2025.128372>
23. H. E. Pace, N. J. Rogers, C. Jarolimek, V. A. Coleman, C. P. Higgins and J. F. Ranville, *Anal. Chem.*, 2011, **83**, 9361–9369. <https://doi.org/10.1021/ac201952t>
24. A. Williams and D. Beauchemin, *Anal. Chem.*, 2020, **92**, 12778–12782. <https://doi.org/10.1021/acs.analchem.0c01415>
25. R. P. Lamsal, G. Jerkiewicz and D. Beauchemin, *Anal. Chem.*, 2016, **88**, 10552–10558. <https://doi.org/10.1021/acs.analchem.6b02656>
26. A. Williams and D. Beauchemin, *J. Anal. At. Spectrom.*, 2022, **37**, 727–732. <https://doi.org/10.1039/D1JA00457C>
27. F. Ardini, M. Grotti, R. Sánchez and J. L. Todolí, *J. Anal. At. Spectrom.*, 2012, **27**, 1400–1404. <https://doi.org/10.1039/C2JA30152K>
28. R. Sánchez, C. Sánchez, J. L. Todolí, C.-P. Lienemann and J.-M. Mermet, *J. Anal. At. Spectrom.*, 2014, **29**, 242–248. <https://doi.org/10.1039/C3JA50146A>
29. S. Martínez, R. Sánchez and J.-L. Todolí, *J. Anal. At. Spectrom.*, 2022, **37**, 1032–1043. <https://doi.org/10.1039/D2JA00024E>
30. D. Wang, J. Zhang, C. Fan, X. Li, L. Liu, X. Yan, Y. Li, B. He, Y. Yin, L. Hu and G. Jiang, *Anal. Chem.*, 2025, **97**, 1792–1798. <https://doi.org/10.1021/acs.analchem.4c05614>
31. H. Wang, M. Wang, B. Wang, L. Zheng, H. Chen, Z. Chai and W. Feng, *Anal. Bioanal. Chem.*, 2017, **409**, 1415–1423. <https://doi.org/10.1007/s00216-016-0075-y>
32. X. Wang, P. Tang, H. Liu, Y. Li, H. Guo, P. Li, D. Han, N. Liu, L. Liu, B. He, L. Hu and G. Jiang, *Anal. Chim. Acta*, 2025, **1380**, 344787. <https://doi.org/10.1016/j.aca.2025.344787>
33. A. Asfaw, W. R. MacFarlane and D. Beauchemin, *J. Anal. At. Spectrom.*, 2012, **27**, 1254–1263. <https://doi.org/10.1039/c2ja30041a>
34. Z. Zhou, A. Al Hejami, M. J. Burgener, J. Burgener and D. Beauchemin, *J. Anal. At. Spectrom.*, 2022, **37**, 1450–1454. <https://doi.org/10.1039/D2JA00059H>
35. Z. Zhou, M. J. Burgener, J. Burgener and D. Beauchemin, *J. Anal. At. Spectrom.*, 2024, **39**, 2078–2086. <https://doi.org/10.1039/D4JA00075G>

36. Z. Liu, A. Xue, H. Chen and S. Li, *Appl. Microbiol. Biotechnol.*, 2019, **103**, 1475–1483. <https://doi.org/10.1007/s00253-018-09587-w>
 37. H. Tanguler and H. Erten, *Food and Bioproducts Processing*, 2008, **86**, 317–321, <https://doi.org/10.1016/j.fbp.2007.10.015>
 38. A. Horvath and H. Riezman, *Yeast*, 1994, **10**, 1305–1310, <https://doi.org/10.1002/yea.320101007>
 39. RA. Ribeiro, N. Bourbon-Melo, I. Sá-Correia. *Front Microbiol.* 2022, **13**, 953479. <https://doi.org/10.3389/fmicb.2022.953479>
 40. J. H. T. M. Fabri, N. P. de Sá, I. Malavazi and M. Del Poeta, *Prog. Lipid Res.*, 2020, **80**, 101063. <https://doi.org/10.1016/j.plipres.2020.101063>
-